THE ASTROPHYSICAL JOURNAL, 466:704–712, 1996 August 1

REVERBERATION MAPPING AND THE DISK-WIND MODEL OF THE BROAD-LINE REGION

J. CHIANG AND N. MURRAY
Canadian Institute for Theoretical Astrophysics, McLennan Laboratories, 60 Saint George Street, Toronto, Ontario, Canada, M5S 1A1
Received 1995 November 1; accepted 1996 February 12

ABSTRACT

Using the disk-wind model of Murray et al., we calculate line profiles and frequency-resolved response functions for broad-line emission from the surface of an accretion disk in an active galactic nucleus in the presence of a radiatively driven wind. We find that the combined effects of the shears in the wind and in the disk itself produce anisotropic line emission, which solves several well-known problems connected with disk models of the broad-line region. In particular, the broadening of resonance lines such as C IV, Lyα, and N V can be attributed to orbital motion of the disk gas at radii as close as $\sim 10^{16}$ cm in Seyferts, without requiring unrealistically large emission regions in order to produce single-peaked profiles. Furthermore, the anisotropy of the line emission results in frequency-dependent response functions which are no longer red-blue symmetric, so that the time delays inferred for the various red and blue components of the line agree qualitatively with recent reverberation mapping observations of NGC 5548.

Subject headings: accretion, accretion disks — galaxies: active — galaxies: Seyfert — line: profiles — quasars: emission lines

1. INTRODUCTION

Broad emission lines (BELs) are the distinguishing feature of the spectra of active galactive nuclei (AGNs), and the variability, absorption, profile shape, and strength of these lines are our most powerful probes of their inner structure. The basic photoionization model and the evidence for variability in both the lines and continuum fluxes of AGNs led Blandford & McKee (1982) to propose "reverberation mapping" as a means of constraining the geometry and kinematics of the broad-line region (BLR). The principal underlying reverberation mapping is that the light curve of a given line, $L(t)$, can be related to the continuum light curve, $C(t)$, by a causal, linear transformation. The frequency-dependent version of this transformation is

$$L(t, v) = \int_0^{+\infty} \psi(\tau, v) C(t - \tau) d\tau \,, \qquad (1)$$

where the transfer function $\psi(\tau, v)$ is the emission-line response to a δ-function outburst of the ionizing continuum. In principle, the convolution theorem and Fourier inversion can be used to determine $\psi(\tau, v)$ from data. The actual geometry and velocity structure of the BLR can then be inferred from some model for the kinematics of the BLR and from the fact that the surfaces of constant delay are paraboloids aligned along the observer line of sight with the central continuum source at the focus.

The difficulties associated with actually performing such an inversion have motivated long-term observations of AGNs in order to obtain high-quality spectra and light curves. The first of these extensive monitoring programs was the combined *IUE*/ground-based observations of NGC 5548 in 1988–1989 (Clavel et al. 1991). Several major insights into the BLR resulted from the analysis of these NGC 5548 observations. First of all, the BLR was found to be substantially more complicated than the earlier models based on single-zone photoionization calculations had assumed. From the structure of the response functions, Krolik et al. (1991) concluded that the BLR in NGC 5548 extends over a large range of radii, with the inner radius being much smaller than previously inferred. Furthermore, cross-correlation analysis of light curves of various lines with the continuum has shown that the BLR is stratified: longer lag times were found for lower ionization lines, such as Hβ and C III, than for higher ionization lines, such as N V, C IV and He II (Clavel et al. 1991). Also, because of the higher quality spectral data, the response functions of separate components of a single line could be studied. Crenshaw & Blackwell (1990) found evidence for a faster response from the redshifted half of the C IV line versus the blueshifted half. The complexity of the BLR that these studies revealed called for even better data.

The recent *HST*/*IUE*/ground-based effort to monitor NGC 5548 (Korista et al. 1995, hereafter K95) has produced the highest quality data yet obtained for probing the BLR via reverberation mapping techniques. While K95 found that there is very little difference between the response of the red and blue cores of the C IV line, they have found evidence for more rapid responses relative to the cores in the wings of the line, particularly the red wing. They also found indications that the red wing response leads the blue wing response, though because of possible contamination of the red wing by He II, they could not make a definitive conclusion as to the origin of these timing differences.

The most direct evidence of these effects has been obtained by examining the cross-correlation of the emission-line light curves with the continuum, and this was the method employed by K95 on the C IV line of NGC 5548. Recently, efforts have been made toward deconvolutions of the actual line response functions, using various techniques (Horne 1994; Pijpers & Wanders 1994; Krolik & Done 1995). Underscoring the importance of modeling, "echo images" in the τ–v plane for various models of the BLR (including Keplerian disks and spherically symmetric models with radial infall or outflow) have been produced, anticipating frequency-resolved response function deconvolutions (Welsh & Horne 1991; Perez, Robinson, & de la Fuente 1992). Wanders et al. (1995) and Done & Krolik (1996) have made the first attempts at such a deconvolution for the C IV line of NGC 5548. Following K95, they divided

the line into four frequency bands—two "core" components and two "wing" components; they derived separate response functions for each, confirming the cross-correlation results of K95, and they were able to study specific BLR models in greater detail.

Current thinking about the BLR has been dominated for the past decade by the cloud picture (for a review, see Peterson 1994). In these models, dense clouds, appropriately distributed in velocity, are photoionized by the central continuum and emit the line photons that form the broad lines. Since there is very little agreement about how such clouds are formed, how they are confined, and how they attain their velocity distribution, cloud models have the advantage of considerable flexibility in describing the observations. Reverberation mapping and photoionization models have placed some constraints on the nature of the BEL cloud region: the characteristic inner radius of the C IV BLR is likely ~ 3–10 light-days; the clouds are almost certainly optically thick, though the absence of Lyman edges suggests that individual clouds are significantly smaller than the size of the central continuum emitting region; the smoothness of the line profiles implies that there are of order more than 10^5 clouds contributing to any given line profile. Finally, the faster response times for the red wing of the C IV line of NGC 5548 versus the blue wing imply that any radial motion that the clouds possess must be predominantly inward rather than away from the central source.

It is this last feature that has led some to dismiss the disk model of the BLR. Because the velocity field in a disk, which is usually taken to be Keplerian, is symmetric with respect to redshifted and blueshifted emission, it is expected that the timing response for both sides of the line should also be symmetric (Done & Krolik 1996). However, this is only necessarily the case if the line emission from the surface of the disk is *isotropic*, as is generally assumed (Welsh & Horne 1991; Dumont & Collin-Souffrin 1990; Blandford & McKee 1982). In this work, we show that in the disk-wind model of Murray et al. (1995, hereafter M95), the combination of the shears in a Keplerian disk and a radiatively driven disk wind produces an anisotropic opacity for the line emission. This emission anisotropy has several important consequences: it solves the double-peak problem of disk line profiles (Mathews 1982) without requiring unrealistically large BLR radii; it provides a natural explanation for the faster response of the redshifted line emission despite the symmetry in the disk velocity structure; and it establishes a connection with the observed blueshifted absorption in the C IV line of NGC 5548 and the disk-wind models of broad absorption line QSOs. Furthermore, this model for the BLR allows the mass of the central object to be constrained, and thus provides additional evidence for the massive black hole hypothesis for the centers of AGNs.

The plan for the remainder of this paper is as follows. In § 2, we review the disk-wind model of M95, discuss its observational connection with warm absorbers and Seyfert galaxies, derive the expressions for computing time-averaged line profiles, and compare a model line profile with data from NGC 5548. In § 3, we derive the frequency-resolved response functions, discuss how the red/blue timing asymmetry arises, apply our calculations to the NGC 5548 data, and compare our results with the deconvolved response functions of Done & Krolik (1996) and Wanders et al. (1995). In § 4, we discuss some observational consequences of our model, address possible objections, and discuss prospects for more detailed work in the future. Finally, we summarize our conclusions in § 5.

2. THE DISK-WIND MODEL

Our model for the BEL region of AGNs is based upon the broad absorption line (BAL) QSO model of M95. In BAL QSOs, the broad-line spectra are similar to that of ordinary QSOs except for the deep, broad absorption troughs blueward of line center. Based on this similarity, Weymann et al. (1991) have concluded that ordinary QSOs and BAL QSOs belong to the same class of object—only the observer's line of sight to the central source distinguishes them, passing through absorbing material for the latter objects. Because some of the line emission is also absorbed, the cloud picture requires that two distinct sets of clouds exist in the BLR. The broad emission-line clouds exist at the inner radii, closer to the central continuum, while the BAL clouds surround them, with an appropriate covering factor to account for the absorption-line profiles.[1]

The complexities and difficulties associated with cloud models of BAL QSOs led M95 to consider a different approach. Noting the similarity in the BAL profiles to the P Cygni profiles found in O star spectra, they considered the possibility that a radiatively driven wind provides the observed absorption. In O stars, it has been well established that such winds are responsible for the shape of the resonance lines (Castor, Abbott, & Klein 1975; Pauldrach et al. 1994). Following the formalism of Castor et al. (1975) for radiatively driven winds, M95 calculated the dynamics of a wind that is driven from the surface of an accretion disk. They found that the velocity and ionization structure of these winds can account for the width and shape of the absorption troughs as well as providing a natural explanation for the inferred covering factor ($\sim 10\%$) of the BAL region. The relevance of this model for lower luminosity AGNs became more clear when a connection was established between the discovery in X-rays of photoionized bulk outflows, the so-called "warm absorbers" (Turner et al. 1993; Mathur et al. 1994) in Seyfert galaxies, and the presence of blueward absorption features in resonance line spectra in these same objects (Murray & Chiang 1995). These results suggest that radiatively driven winds may be a ubiquitous feature of all AGNs. Since broad emission lines are also universal, it is natural that a connection exists between them as well.

In order to illustrate the applicability of the disk-wind model to the broad emission-line region, we consider a simplified description of the velocity structure of the wind. The wind consists of nearly radial streamlines, which have origins, or footpoints, at various radii on the surface of the disk. Near the footpoint radius, r_f, for a given streamline, the gas is initially driven upward by the surface radiation of the disk. At a vertical height, which is approximately the scale height of the disk, the radiation pressure from the central continuum source becomes strong enough to push the gas predominantly radially outward. M95 have integrated the equations of motion using the radiation force law, determined from calculations using the photoionization code CLOUDY (Ferland 1993) and the line list of

[1] Various descriptions of cloud models for BEL and BAL regions can be found in Arav, Li, & Begelman (1994) and Emmering, Blandford, & Shlosman (1992) and references therein.

Verner, Barthel, & Tytler (1994). They found that the radial component of the gas velocity along a streamline can be described approximately by

$$v_r(r) = v_\infty\left(1 - \frac{r_f}{r}\right)^\gamma , \tag{2}$$

where the terminal velocity of the streamline, v_∞, is within factors of order unity of the local escape velocity, $v_{esc} = (2GM/r_f)^{1/2}$, and the exponent $\gamma \simeq 1.0$–1.3. It should be noted that this exponent differs from the result for O stars ($\gamma \simeq 0.5$; Castor et al. 1975) because of the differing force multiplier law, as derived from the photoionization calculations, and the importance of the centrifugal support of the rotating Keplerian disk. In the following discussion, we will use $\gamma = 1$.

M95 have performed dynamical and photoionization calculations that show that the inner edge of the wind should be located at $\sim 3 \times 10^{15}$ cm for an accretion disk around a $10^7\ M_\odot$ black hole. It is important to note that at these radii, the shear in the disk itself is sufficient to make the Sobolev approximation an appropriate description of the resonance line transfer in the disk (cf. Castor 1970). Murray & Chiang (1996) discuss the validity of this approximation in greater detail. For our purposes, it is sufficient to note that the Sobolev length scale associated with the shear due to the differential rotation of the disk is

$$l_S \sim \frac{v_{th}}{v_\phi/r} , \tag{3}$$

where $v_{th} \sim 10^6$ cm s^{-1} is the thermal velocity of the disk gas and $v_\phi = (GM/r)^{1/2}$ is the azimuthal disk velocity. The relevant length scale for the Shakura-Sunyaev thin-disk solution (Shakura & Sunyaev 1973) is $l_{disk} \sim v_s/(v_\phi/r)$, where v_s is the sound speed and is determined by gas pressure in the disk. Comparing these two quantities, we have

$$\frac{l_S^2}{l_{disk}^2} = \frac{v_{th}^2}{v_s^2} \tag{4}$$

$$= \frac{p_{gas}}{p_{rad}} \ll 1 \tag{5}$$

for the radiation pressure-supported part of the disk, where p_{gas} and p_{rad} are the gas pressure and radiation pressure, respectively. This implies that, as within the wind itself, the Sobolev approximation also applies to the disk.

We expect that the largest contribution to the line emission will be from regions of high density. Therefore, we will assume for now that the line emission originates primarily near the wind footpoints at the surface of the accretion disk where the densities are high ($n_H \sim 10^9$ cm^{-3}), but the continuum optical depths, which are largely due to electron scattering, are still no more than order unity. At these locations, the velocity of the gas is composed of a radial component due to the wind and an azimuthal component due to the disk motion:

$$\boldsymbol{v} = v_r\hat{\boldsymbol{r}} + v_\phi\hat{\boldsymbol{\phi}} . \tag{6}$$

For an observer located in the y–z plane with a line-of-sight angle i with respect to the disk symmetry axis (see Fig. 1), the projected velocity shift at a location (r, ϕ) on the disk is

$$v_{proj} = \sin i(v_r \sin\phi + v_\phi \cos\phi) . \tag{7}$$

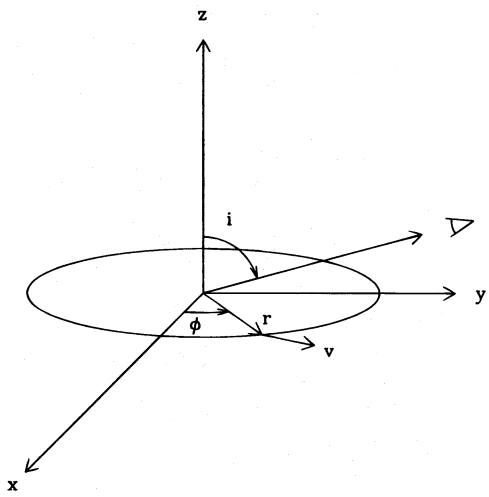

FIG. 1.—Geometry of the disk broad-line region. The angle, i, is the disk inclination relative to the observer. The quantities (r, ϕ) label locations on the disk.

Note that we have neglected the finite thickness of the disk ($\sim 10^{13}$ cm), which is much smaller than the inferred radius of the BLR ($\sim 10^{16}$ cm).

Because of the azimuthal symmetry of the problem, we model the line source function, $S(r)$, to be a function only of the disk radius. The contribution to the line profile at a given frequency is

$$L_\nu = \cos i \int_{r_{min}}^{r_{max}} r\,dr \int_0^{2\pi} d\phi k(r)S(r)\frac{1 - e^{-\tau}}{\tau}\,\delta[\nu - \tilde{\nu}(\phi, r)] , \tag{8}$$

where r_{min} and r_{max} are the radial boundaries of the BLR, $\tilde{\nu}$ is the Doppler-shifted frequency of the line at the disk element, which has velocity v_{proj}:

$$\tilde{\nu} = \nu_0\left(1 + \frac{v_{proj}}{c}\right) , \tag{9}$$

and ν_0 is the frequency of the line.[2] The optical depth τ is angle dependent and is *locally* determined in the Sobolev approximation, and $k(r)$ is the integrated line opacity (Rybicki & Hummer 1983). In the notation of Hamann, Korista, & Morris (1993), the quantity

$$\beta(r, \phi, i) = \frac{1 - e^{-\tau}}{\tau} \tag{10}$$

is known as the *directional* escape probability. Transforming the δ function and evaluating the ϕ integral, we obtain for the integrand of equation (8)

$$\frac{dL_\nu}{dr} = rk(r)S(r)\cos i \left|\frac{d\tilde{\nu}}{d\phi}\right|^{-1} \beta(r, \phi, i) \tag{11}$$

$$= \frac{c}{\nu_0}\frac{rk(r)S(r)}{\tan i\,|v_r\cos\phi - v_\phi\sin\phi|}\beta(r, \phi, i) , \tag{12}$$

where ϕ satisfies $\tilde{\nu}(r, \phi) = \nu$ for a given radius r.

[2] Note that the source function $S(r)$ in eq. (8) differs from the usual definition in that it contains an implicit integral in the z direction. Its units are ergs s^{-1} cm^{-1} sr^{-1} (cf. Rybicki & Hummer 1978).

The line optical depth in the Sobolev approximation is

$$\tau = \frac{\kappa \rho v_{\rm th}}{|\hat{\boldsymbol{n}} \cdot \boldsymbol{\Lambda} \cdot \hat{\boldsymbol{n}}|}, \tag{13}$$

where κ is the line absorption coefficient, ρ is the density, $\hat{\boldsymbol{n}}$ is the line-of-sight vector to the observer, and Λ is the symmetric strain tensor (Castor 1970; Rybicki & Hummer 1978). For the C IV line, the line absorption coefficient is

$$\kappa \simeq 2.61 \times 10^7 \eta_{\rm C+3}, \tag{14}$$

assuming a cosmic abundance of carbon, and where $\eta_{\rm C+3}$ is the fractional abundance of the C^{+3} ion. We expect $\eta_{\rm C+3}$ to be of order unity throughout the C IV broad emission line region. For the velocity structure given by equations (2) and (6), we have

$$\begin{aligned}\hat{\boldsymbol{n}} \cdot \boldsymbol{\Lambda} \cdot \hat{\boldsymbol{n}} = \sin^2 i \Bigg[& \frac{\partial v_r}{\partial r} \sin^2 \phi \\ & + \left(\frac{\partial v_\phi}{\partial r} - \frac{v_\phi}{r} \right) \sin \phi \cos \phi + \frac{v_r}{r} \cos^2 \phi \Bigg] \\ & - \sin i \cos i \left(\frac{1}{r} \frac{\partial v_r}{\partial \theta} \sin \phi + \frac{1}{r} \frac{\partial v_\phi}{\partial \theta} \cos \phi \right) \\ & + \frac{v_r}{r} \cos^2 i . \end{aligned} \tag{15}$$

For high inclinations, the term proportional to $\sin^2 i$ will dominate, while for lines of sight closer to the accretion disk symmetry axis, the term proportional to $\sin i \cos i$ will be the important term.

We use a disk inclination angle $i = 75°$ in this calculation for NGC 5548. This choice is motivated by the presence of the warm absorber and the expectation that it is due to a highly ionized component of the disk wind that lies in the observer line of sight (Murray & Chiang 1995). Since in this case $\sin i \gg \cos i$, we will only consider the term proportional to $\sin^2 i$ in equation (15) in the following discussion (cf. Murray & Chiang 1996). The results remain qualitatively the same for the full expression.

The equation for the shear in the wind then becomes

$$\begin{aligned}\hat{\boldsymbol{n}} \cdot \boldsymbol{\Lambda} \cdot \hat{\boldsymbol{n}} = & \sin^2 i \\ & \times \left(v_\infty \frac{r_f}{r^2} \sin^2 \phi - \frac{3}{2} \frac{v_\phi}{r} \sin \phi \cos \phi + \frac{v_r}{r} \cos^2 \phi \right). \end{aligned} \tag{16}$$

Evaluated at the high-density regions near the footpoints of the wind streamlines, this factor is of order $\sim v_\phi / r_f$. Combining equations (13), (14), and (16), the optical depth in the line is of order

$$\tau \sim 10^5 \frac{n_{\rm H}}{10^9 \ {\rm cm}^{-3}}; \tag{17}$$

so we can use

$$\beta \simeq \frac{1}{\tau}. \tag{18}$$

The final expression for the luminosity per unit radius is

$$\begin{aligned}\frac{dL_\nu}{dr} = & rS(r) \sin i \cos i \\ & \times \left| \frac{(\partial v_r / \partial r) \sin^2 \phi - (3/2)(v_\phi / r) \sin \phi \cos \phi + (v_r / r) \cos^2 \phi}{v_r \cos \phi - v_\phi \sin \phi} \right| \end{aligned} \tag{19}$$

$$\simeq S(r) \sin i \cos i \left| \left(\frac{v_\infty}{v_\phi} \sin \phi - \frac{3}{2} \cos \phi \right) \right|, \tag{20}$$

where the final form is obtained by evaluating equation (19) near the wind streamline footpoints, $r \simeq r_f$, and neglecting terms that are proportional to $v_r / v_\phi \lesssim 10^{-2}$. We note that the remaining r dependence is contained in the source function $S(r)$, given that v_∞ and v_ϕ both scale as $r^{-1/2}$.

It is not entirely clear how the central continuum source illuminates the outer regions of the disk where the broad emission lines are formed. The standard picture of AGNs is that the UV and X-ray continua are emitted from the hot inner regions of the accretion disk. However, the Shakura-Sunyaev thin disk solution, which is thought to apply to these inner regions, gives a disk height that is essentially constant from the hot inner regions out to the disk BLR. Therefore, in the standard thin-disk solution, there would not be any lines of sight from the continuum source to the BLR. However, in disk models of the BLR, it is conventional to assume either that a continuum source exists a moderate distance above the inner regions of the disk (Matt, Fabian, & Ross 1993) or that there is a hot, spherical region at the center of the disk (Rokaki & Magnan 1994). In any case, for the purposes of the reverberation mapping study, we will assume that there is a central source of ionizing continuum that is situated not far above the disk plane [$z \sim 10^{13} (M/10^7 \ M_\odot)$ cm], and that can illuminate the disk BLR.

In order to reproduce a reasonable line profile shape (cf. Fig. 2), we have found that the radial dependence in equation (20) can be adequately modeled by

$$S(r) \propto r^{-\alpha}, \tag{21}$$

with a value of $\alpha \simeq 1$. The inner radial boundary of the BLR, $r_{\rm min}$, is constrained by the reverberation mapping results and photoionization calculations. The outer radial boundary, $r_{\rm max}$, is determined by the location of the Strömgren radius for the ion in question. Preliminary photoionization results give $r_{\rm max} \sim 10^2 r_{\rm min}$ for the C IV line in NGC 5548. Using this radial dependence and these boundaries, we have integrated equation (8), and we find the line profile (*solid line*) for C IV shown in Figure 2. For comparison, the dashed line is the mean FOS C IV line profile of NGC 5548 from the recent *HST* observations (K95), and the dot-dashed line results from the same model calculation except that isotropic emission is assumed. The effect of the anisotropic optical depth is clear: the disk-wind shears result in single-peaked profiles, and the shape of the line, except for the blueward absorption and a possible contribution from a narrow-line component, are well-matched.

It should also be noted that these results only apply to the *shape* of the line from our model. Accordingly, the model lines shown in Figure 2 are normalized so that their equivalent widths match that of the observed line. For a full comparison with the data to be made, more complete

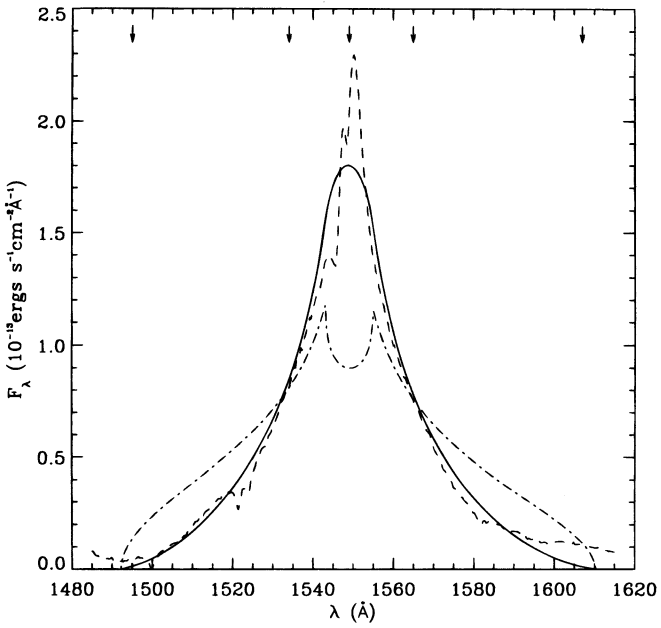

FIG. 2.—Data and model line profiles for the C IV line of NGC 5548. The solid line is the model calculation including the effects of the anisotropic emission. The dashed line is the data from the 1994 *HST* observations described by Korista et al. (1995). Also shown is the double-peaked profile (*dot-dashed line*) of a model line calculation that assumes isotropic emission. The arrows indicate the boundaries of the various wing and core components.

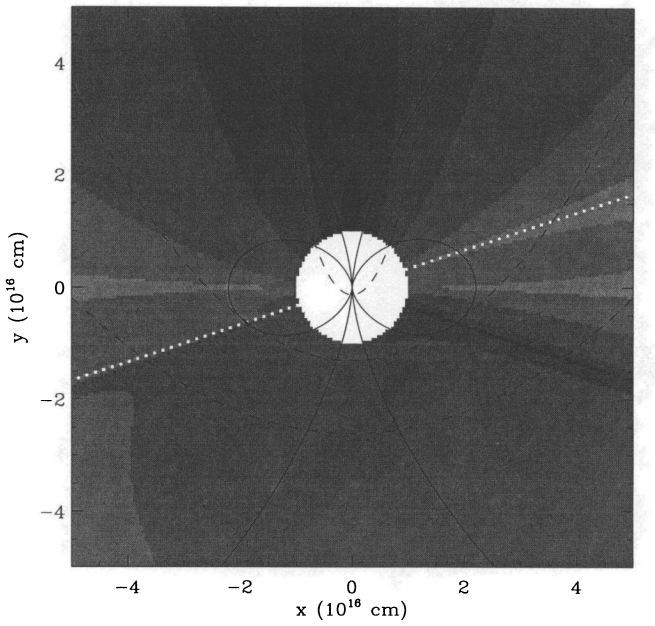

FIG. 3.—Disk map of the line transfer function ψ. Darker areas indicate stronger emission, and the diagonal line of white pixels corresponds to the locus of weakest emission. The solid lines are the lines of constant frequency, indicating the boundaries of the blue and red wing components. They are at 10,840 km s^{-1} (*right side, inner curve*), 3000 km s^{-1} (*right side, outer curve*, which extends beyond the plot boundaries), -3000 km s^{-1} (*left side, outer curve*) and $-10{,}840$ km s^{-1} (*left side, inner curve*). The dashed lines are the lines of constant time delay at $\tau = 0.5$, 5, and 10 days.

photoionization calculations would have to be performed using the detailed disk-wind velocity and ionization structure and the actual ionizing continuum of NGC 5548. The preceding arguments are presented to show that the scalings we have inferred are reasonable and that there is physical motivation for the disk-wind model.

3. DISK-WIND RESPONSE FUNCTION

Thus far, the line profiles we have presented are for a steady continuum source. We now derive the transfer function in order to consider variability. We have

$$\psi(\tau, v) = \int_{\rm disk} dA k(r) S(r) \beta(r, \phi, i) \delta[\tau - \tilde{\tau}(r, \phi)] \delta[v - \tilde{v}(r, \phi)]$$
$$= \int r\, dr \int d\phi k(r) S(r) \beta(r, \phi, i) \delta(\tau - \tilde{\tau}) \delta(v - \tilde{v}) \,. \quad (22)$$

For each point on the disk, (r, ϕ), there is associated a time delay and frequency, (τ, v). Transforming the integral over the disk area to one over τ and v, we obtain

$$\psi(\tau, v) = \left| \frac{r k(r) S(r) \beta(r, \phi, i)}{|(\partial\tau/\partial r)(\partial\tau/\partial\phi) - (\partial\tau/\partial\phi)(\partial v/\partial r)|} \right|_{\substack{r = \tilde{r}(\tau, v) \\ \phi = \tilde{\phi}(\tau, v)}} . \quad (23)$$

The denominator is the Jacobian of the transformation, and the entire expression is evaluated at the corresponding locations $(\tilde{r}, \tilde{\phi})$ on the disk that yield the desired time delay and frequency. Figure 3 is an image depicting the value of the transfer function as a function of location on the disk (cf. Fig. 1). Also plotted are the lines of constant time delay (*dashed lines*) and the lines of constant frequency (*solid lines*), in order to illustrate the mapping from (r, ϕ) to (τ, v).

The lines of constant time delay are given by the intersection of the constant time delay paraboloids and the disk surface. Near the disk surface, the radial component of the velocity, $v_r \sim 10^7$ cm s^{-1}, is small compared with the azimuthal velocity, $v_\phi \sim 10^8$–10^9 cm s^{-1}, throughout the BLR. Therefore, the projected velocity (cf. eq. [7]) is approximately

$$v_{\rm proj} \simeq \sqrt{\frac{GM}{r}} \sin i \cos\phi \,, \quad (24)$$

so that for a given frequency shift Δv, we have

$$r \simeq \frac{GM \sin^2 i}{v_{\rm proj}^2} \cos^2\phi \,. \quad (25)$$

From this expression, we see that the loci of constant absolute shift $|\Delta v|$ look like lobes that are nearly red-blue symmetric.

The red-blue asymmetry of the disk response function can be attributed to the radiative transfer effects due to the radial and azimuthal shear of the disk wind. From equation (20), we see that the ϕ-dependence of the disk contribution to the line luminosity is

$$\frac{dL_v}{dr} \propto \left| \frac{v_\infty}{v_\phi} \sin\phi - \frac{3}{2} \cos\phi \right| . \quad (26)$$

Because $v_\infty \sim v_\phi$ and both are intrinsically positive quantities, the transfer function attains small values near the median angles ($\sim 45°$, 270°) in the upper right and lower left quadrants of the disk, as shown in Figure 3. These smaller values of the emission seen by the observer are depicted by

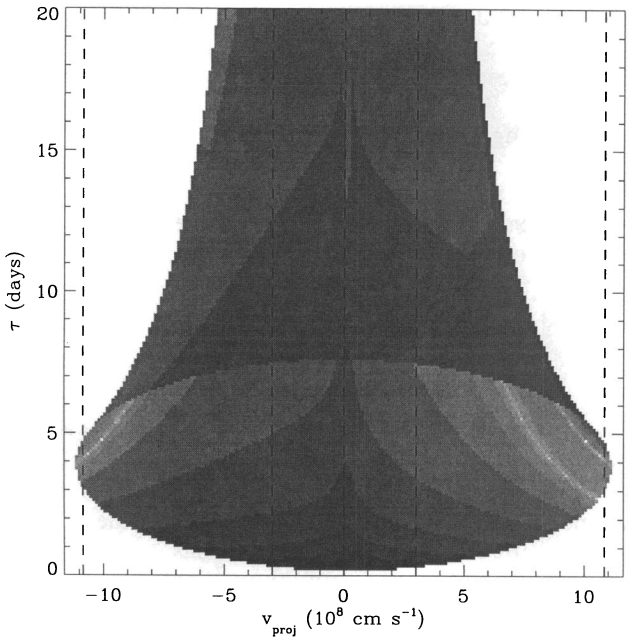

FIG. 4.—Echo image of the transfer function in (v_{proj}, τ) space. Dashed lines are the boundaries of the various line components.

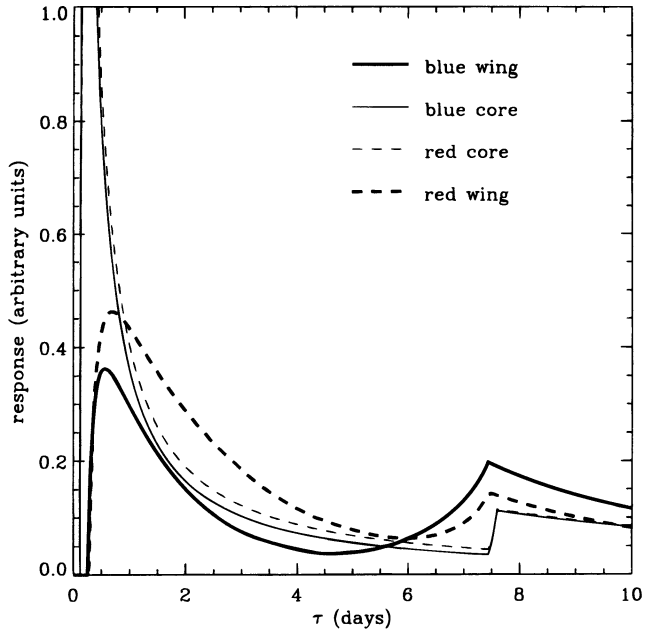

FIG. 5.—Model response functions for the various components of the C IV line.

the lighter pixels in the image. Figure 4 is an echo image of the response function in (τ, v) space; note the similarities and differences with respect to the echo image maps for disk BLR models with isotropic emission given in Welsh & Horne (1991) and Perez et al. (1992).

Following K95, we consider the timing response for the blue/red wing and core components of the C IV line. The core components are defined to extend from Doppler shifts of 0 to ± 3000 km s^{-1} and the wing components from ± 3000 to 10,840 km s^{-1}. The small arrows in Figure 2 indicate these boundaries at the corresponding wavelengths. We have integrated equation (23) over frequency for these four bands and found the response functions shown in Figure 5. As with the response functions found by the deconvolutions (Done & Krolik 1996; Wanders et al. 1995), the core components are nearly identical and are very similar to the blue wing component, except at very short timescales ($\lesssim 1$ day). Most significantly, the red wing has significantly stronger response at shorter timescales (~ 1–4 days) than the other three components. In addition, the secondary peaks found by both Wanders et al. (1995) and Done & Krolik (1996) at delays of 8–15 days are also a natural consequence of the disk model.

The faster response of the red wing can be understood by considering Figure 3. The blue and red wing frequency ranges are bounded by the solid lines, and the 0.5, 5, and 10 day time delay lines are indicated by the dashed lines. Within the earlier region, between 0.5 and 5 days, the red wing response is stronger than the response of the blue wing. This occurs because the locations of weaker emission due to the near cancellation of two ϕ-dependent terms in equation (26) pass through the blue wing region but not through the corresponding red wing region. At later times, from 5 to 10 days, the situation is reversed—the line of near cancellation of the ϕ-dependent terms now passes predominantly through the red wing region and does not suppress as much emission in the corresponding blue region. In effect, the response in the blue wing "catches up" to and surpasses that of the red wing—this is evident in the second peak of the blue wing response function at ~ 8 days. In Figure 4, the difference in the red and blue response functions can also be clearly seen.

In order to underscore the applicability of this model to actual data, we have used the combined *IUE*/*HST* spectra of K95 to create light curves for the four line components and cross-correlation functions of these model light curves with the continuum. Figure 6 shows the 1350 Å continuum (mean subtracted) as measured by *IUE* (SWP) and *HST*

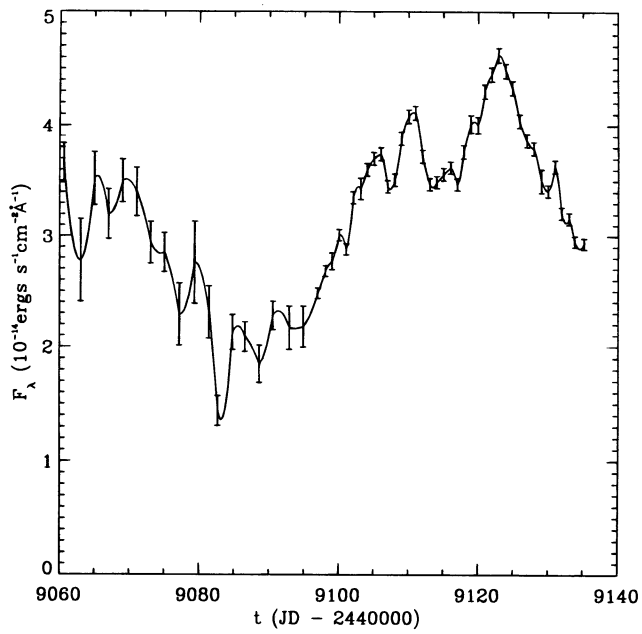

FIG. 6.—Continuum at 1350 Å of NGC 5548. Plotted points are the data as measured by *IUE* and *HST* (Korista et al. 1995), and the solid curve is the interpolated function we have used in our cross-correlation analysis.

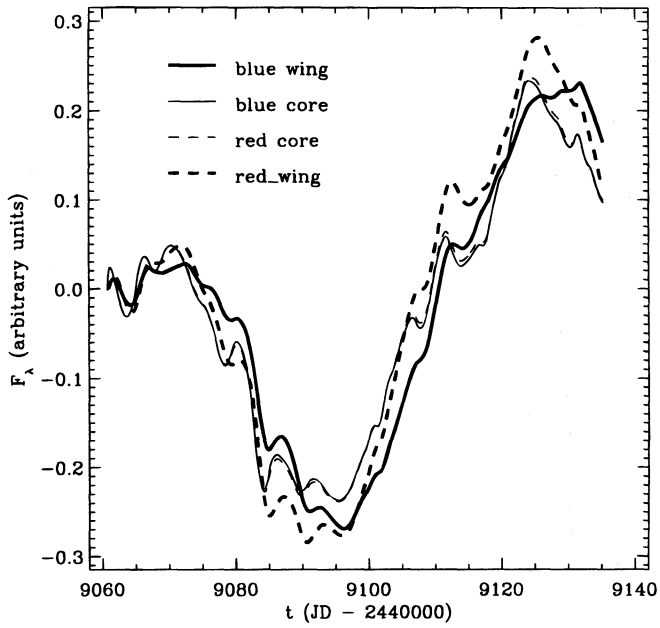

FIG. 7.—Model light curves of the various components of the C IV line of NGC 5548.

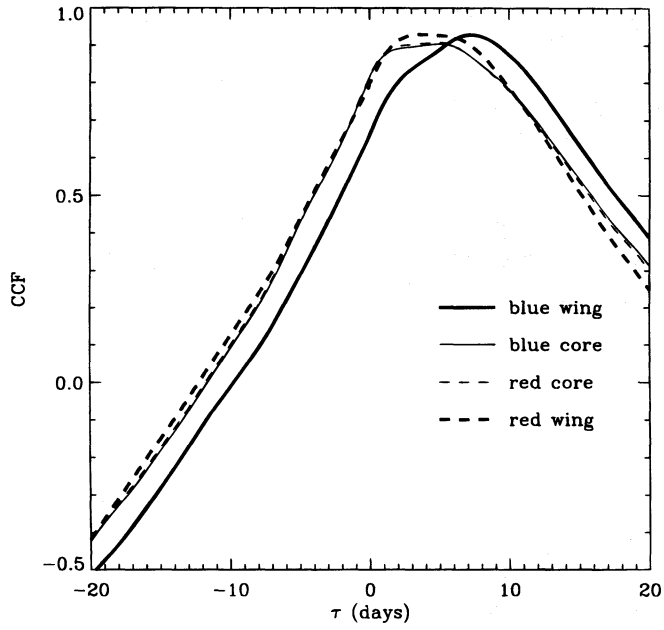

FIG. 8.—Cross-correlation functions for the four components of the C IV line with the 1350 Å continuum.

TABLE 1

CROSS-CORRELATION RESULTS

C IV Component	Disk-Wind Model		*HST* Observations (K95)	
	Δt_{peak} (days)	$\Delta t_{centroid}$	Δt_{peak}	$\Delta t_{centroid}$
Blue wing.....	7.2	6.0	7.5	8.3
Blue core	5.0	4.3	...	...
Red core.....	4.9	4.3	...	...
Red wing	3.6	4.4	3.5	4.3

over an ~80 day period. The solid line is the interpolated continuum we have used for the convolutions, and Figure 7 shows the resulting light curves for each of the four line components. The earlier response of the red wing relative to the blue wing is clearly evident. Figure 8 shows the cross-correlation functions for these light curves with the interpolated 1350 Å continuum (cf. Figure 15 in K95). Table 1 lists the peak and centroid values of the inferred lags for each component.

4. DISCUSSION

4.1. *Response Function Structure and Line Profile Variations*

The detailed structure of the frequency-resolved response functions may also be useful in explaining asymmetries in the broad-line profiles, as well as long-term variability in the line structure. The larger second peak in the blue-wing response at ~8 days may either "alias" or "antialias" structure present in the continuum light curve into the mean line profile for a typical observation. The result would be line profiles that would be skewed toward either the blue or the red, depending on the phase and strength of the continuum light curve variations relative to the time window(s) of the observation. On the other hand, Perry, van Groningen, & Wanders (1994) have shown that the variations seen in the shape of the C IV line of NGC 4151 are preceded by similar continuum light curves. They argue that the changes in the line shape may instead be due to structural changes in the BLR, an extended or anisotropic continuum source, or a significantly larger BLR than that deduced from cross-correlation analysis. In any case, the structure of the response functions will still be reflected in the shape of the emission line in the way we have described. If these other effects are not significant, then examining the line profile structure and the preceding continuum variations may be an additional means of discriminating between different kinematic models of the BLR.

4.2. *Constraints on the Mass of the Central Object*

The radial extent of the BLR is determined by the reverberation mapping results, and the velocity field is determined by the width of the resonance lines and the photoionization results for the ionization structure of the disk wind. Thus, the observations essentially fix the quantities r and v_ϕ. The assumption of Keplerian motion relates these two quantities by

$$v_\phi = \sqrt{\frac{GM}{r}}, \tag{27}$$

in such a way that the mass of the central object is actually constrained by these observations. Now, since $M \propto r$ for a fixed line width (i.e., v_ϕ is about constant) and since the lags are related to radii on the disk linearly, $\tau \propto r$, we have

$$M \propto \tau . \tag{28}$$

The lags, which we infer from the cross-correlation functions (Fig. 8 and Table 1), agree with the values given by K95 to within 20%, and we have determined the mass of the central object of NGC 5548 to be $\simeq 10^8\ M_\odot$. Furthermore, for objects with line widths similar to NGC 5548, the observed lags for those lines give a direct measurement of

the mass of the central object if this model for the BLR is correct.

4.3. *Broad Iron* Kα *Lines*

One of the difficulties of this model of the broad-line region is that observations of broad, redshifted iron Kα lines in Seyfert 1's seem to indicate that the disks are being viewed predominantly face-on with inclinations of $i \sim 20°$–$30°$. In these objects, the iron emission is believed to originate near the inner edge of the accretion disk at radii $\sim 3R_S$, where R_S is the Schwarzschild radius of the central black hole (Matt et al. 1993). Mushotzky et al. (1995) report that *Ginga* observations of NGC 5548 have found that the equivalent width of the Fe Kα line is ~ 150 eV and that this is best fit by disk inclinations of $i \sim 15°$–$38°$. On the other hand, as Wanders et al. (1995) and Done & Krolik (1996) have pointed out, in order for the response functions of a disk with inner radius $\sim 10^{16}$ cm to peak near zero delay, the disk must be highly inclined.

We do not believe that these observations of the iron Kα lines and our disk model for the UV BLR are irreconcilable. First, the timing resolution of the NGC 5548 observations is no better than 1 day, and we can still produce response functions with the peak response at time delays less than 1 day for disk inclinations as small as $i \sim 60°$. Second, Mushotzky et al. (1995) state that only three of the five parameters—inner and outer radii of the emitting region, initial line energy, disk inclination, and line flux—that are necessary to describe the iron line are actually constrained by the NGC 5548 data. Third, Tanaka et al. (1995) and Matt et al. (1993) have indicated that the emitting material in the Seyfert 1s may be in a higher ionization state than they have considered and that this can increase the relative yield of Fe Kα photons, thus relaxing the constraint on larger inclination angles. Finally, it should be noted that the constraints that are also based on the *shape* of the Fe Kα, arrived at by Tanaka et al. (1995) for the Seyfert galaxy MCG – 6-30-15, are based upon radiative transfer calculations, which, to our knowledge, ignore the effect of shears in the disk. We have seen that these effects can have a significant impact on the shape of the emission line (cf. Fig. 2) and may also affect the amount of line flux that escapes.

4.4. *Comparison with Other Models*

The models of the BLR described by Wanders et al. (1995) and Done & Krolik (1996) have been parameterized to fit the reverberation mapping data of NGC 5548. By contrast, our model qualitatively fits the timing data with only the black hole mass as a free parameter—the other parameters of our model are fixed either by the dynamics, the X-ray warm absorber observations, or the C IV line profile shape. Higher time resolution monitoring of NGC 5548 that reveals variations on timescales smaller than ~ 1 day may be able to constrain these models further, and thus distinguish between them; but the high signal-to-noise ratio required would likely make such observations very difficult.

A more fruitful observation plan would be to monitor a variety of objects, since the most pronounced differences between the models are a function of the inclination of the AGNs. The model of Done & Krolik (1996) consists of a spherically symmetric, extended BLR in which the clouds have predominantly random velocities with a net tendency toward inward motion. If this model applies universally, then the response function shapes obtained for NGC 5548 should apply equally well to all AGN BLRs, regardless of inclination. Only the distance scaling, which depends on the mass of the central object, should be affected. The model of Wanders et al. (1995) also consists of a spherically symmetric cloud BLR, but the central continuum source is assumed to be anisotropic and illuminates a biconical region of the BLR (with semiopening angle $\sim 30°$–$60°$) in which the line emission forms. This model predicts a dependence on inclination for the response functions and also that double-peaked emission lines should result for observer lines of light that lie outside the biconical region.

In our model, as long as the shear due to the radial outflow is present, the emission lines will be single-peaked, regardless of inclination. For very low inclination objects ($i \lesssim 15°$), the response functions should be zero for delay times less than about the light travel time to the inner BLR radius for a given ion. In moderate inclination objects ($i \sim 45°$–$60°$), depending on the precise kinematics of the wind, the secondary peaks in the response functions may be more prominent than those in higher inclination objects. Timing resolution somewhat better than that of the *HST* NGC 5548 campaign (K95) should be able to detect these features in these lower inclination objects.

4.5. *Future Work*

We have not presented here a detailed model of the line emission from NGC 5548. The photoionization calculations and our simplified model of the disk-wind structure are too crude to be expected to match the observations in detail. Therefore, we have not attempted to fit the NGC 5548 light curves of the C IV components. In order for that to be accomplished, photoionization calculations using a more detailed physical model of the disk-wind structure must be performed. This will enable us to better determine the radial dependence for the emission from each ion and also to probe for nonlinear response of the line emission to the continuum. We would also like to use more realistic velocities and shears in equation (19) and improve the radiative transfer to take into account possible nonlocal effects from multiple resonant Sobolev surfaces (Rybicki & Hummer 1978).

5. CONCLUSIONS

Despite the incompleteness of this model, we have offered a plausible qualitative explanation of the timing response seen in NGC 5548 using a physically motivated model for the BLR. In particular, the response functions we obtain possess many of the features found in the response functions obtained by the deconvolution procedures of Wanders et al. (1995) and Done & Krolik (1996): they peak near zero time delay, the red wing response is stronger than the response of the other components at time delays of ~ 1–4 days, and the secondary peak at 8–14 days is also reproduced. Furthermore, the line profile that we obtain is single-peaked, in agreement with the profiles seen for most broad lines in AGN spectra, and we have shown that by using the width of the line profile and the timing response of the red and blue components, we can estimate the mass of the central black hole—for NGC 5548—to be $\sim 10^8\ M_\odot$.

The most significant finding of this work is that the radiative transfer effects that reproduce the observed line profile and timing response *require* that a wind with large radial

shears be present. Therefore, if it is accepted that the broad lines are produced from the surface of a disk, then something that acts like a radiatively driven wind must exist.

We would like to thank Kirk Korista for generously supplying us with *HST* spectra of NGC 5548, and Chris Done and Julian Krolik for providing us with a manuscript of their work, in advance of publication. We would also like to thank Ignaz Wanders, K. Korista, J. H. Krolik, C. Done, and the anonymous referee for providing us with useful comments, which have greatly improved our presentation. This work was supported by NSERC of Canada and by the Connaught Fund of the University of Toronto.

REFERENCES

Arav, N., Li, Z., & Begelman, M.C. 1994, ApJ, 432, 62
Blandford, R. D., & McKee, C. F. 1982, ApJ, 255, 419
Castor, J. I. 1970, MNRAS, 149, 111
Castor, J. I., Abbott, D. C., & Klein, R. I. 1975, ApJ, 195, 157
Clavel, J., et al. 1991, ApJ, 366, 64
Crenshaw, D. M., & Blackwell, J. H., Jr. 1990, ApJ, 358, L37
Done, C., & Krolik, J. H. 1996 ApJ, 463, 144
Dumont, A. M., & Collin-Souffrin, S. 1990, A&A, 229, 313
Emmering, R.T., Blandford, R.D., & Shlosman, I. 1992, ApJ, 385, 460
Ferland, G. J. 1993, Univ. Kentucky, Depart. Phys. and Astron. Internal Report
Hamann, F., Korista, K. T., & Morris, S. L. 1993, ApJ, 415, 541
Horne, K. 1994, in Reverberation Mapping of the Broad-Line Region in Active Galactic Nuclei, ed. P. M. Gondhalekar, K. Horne, & B. M. Peterson (San Francisco: ASP), 23
Korista, K., et al. 1995, ApJS, 97, 285 (K95)
Krolik, J. H., & Done, C. 1995, ApJ, 440, 166
Krolik, J. H., Horne, K., Kallman, T. R., Malkan, M. A., Edelson, R. A., & Kriss, G. A. 1991, ApJ, 371, 541
Mathews, W. G. 1982, ApJ, 258, 425
Mathur, S., Wilkes, B., Elvis, M., & Fiore, F. 1994, ApJ, 434, 493
Matt, G., Fabian, A. C., & Ross, R. R. 1993, MNRAS, 262, 179
Murray, N., & Chiang, J. 1995, ApJ, 454, L105
———. 1996, ApJ, submitted
Murray, N., Chiang, J., Grossman, S., & Voit, G. M. 1995 ApJ, 451, 498 (M95)
Mushotzky, R., Fabian, A. C., Iwasawa, K., Kunieda, H., Matsuoka, M., Nandra, K., & Tanaka, Y. 1995, MNRAS, 272, L9
Pauldrach, A.W.A., Kudritzki, R.P., Puls, J., Butler, K., & Hunsinger, J. 1994, A&A, 283, 525
Perez, E., Robinson, A., & de la Fuente, L. 1992, MNRAS, 256, 103
Perry, J. J., van Groningen, E., & Wanders, I. 1994, MNRAS, 271, 561
Peterson, B. M. 1994, in Reverberation Mapping of the Broad-Line Region in Active Galactic Nuclei, ed. P. M. Gondhalekar, K. Horne, & B. M. Peterson (San Francisco: ASP), 1
Pijpers, F. P., & Wanders, I. 1994, MNRAS, 271, 183
Rokaki, E., & Magnan, C. 1992, A&A, 261, 41
Rybicki, G. B., & Hummer, D. G. 1978, ApJ, 219, 654
Shakura, N. I., & Sunyaev, R. A. 1973, A&A, 24, 337
Tanaka, Y., et al. 1995, Nature, 375, 659
Turner, T. J., Nandra, K., George, I. M., Fabian, A. C., & Pounds, K. A. 1993, ApJ, 419, 127
Verner, D. A., Barthel, P. D., & Tytler, D. 1994, A&AS, 108, 287
Wanders, I., et al. 1995, ApJ, 453, L87
Welsh, W. F., & Horne, K. 1991, ApJ, 379, 586
Weymann, R. J., Morris, S. L., Foltz, C. B., & Hewett, P. C. 1991, ApJ, 373, 23